Chinese Chemical Letters 36 (2025) 110244

Contents lists available at ScienceDirect

Chinese Chemical Letters

journal homepage: www.elsevier.com/locate/cclet

Synergistic adsorption and singlet oxygenation of humic acid on alkali-activated biochar *via* peroxymonosulfate activation

Huazhe Wang[a], Chenghuan Qiao[a], Chuchu Chen[a], Bing Liu[a], Juanshan Du[b], Qinglian Wu[a], Xiaochi Feng[c], Shuyan Zhan[d], Wan-Qian Guo[a,*]

[a] State Key Laboratory of Urban Water Resource and Environment, Harbin Institute of Technology, Harbin 150090, China
[b] Department of Energy Engineering, Korea Institute of Energy Technology (KENTECH), Naju 58330, South Korea
[c] State Key Laboratory of Urban Water Resource and Environment, School of Civil and Environmental Engineering, Harbin Institute of Technology (Shenzhen), Shenzhen 518055, China
[d] Win Future Environmental Protection Tech. Co., Ltd., Tianjin 300308, China

ARTICLE INFO

Article history:
Received 14 March 2024
Revised 16 June 2024
Accepted 11 July 2024
Available online 14 July 2024

Keywords:
Humic acid
Persulfate
Biochar
Adsorption
Nonradical oxidation

ABSTRACT

Humic acid (HA), as a represent of natural organic matter widely existing in water body, dose harm to water quality and human health; however, it was commonly treated as an environmental background substance while not targeted contaminant in advanced oxidation processes (AOPs). Herein, we investigated the removal of HA in the alkali-activated biochar (KBC)/peroxymonosulfate (PMS) system. The modification of the original biochar (BC) resulted in an increased adsorption capacity and catalytic activity due to the introduction of more micropores, mesopores, and oxygen-containing functional groups, particularly carbonyl groups. Mechanistic insights indicated that HA is primarily chemically adsorbed on the KBC surface, while singlet oxygen ($^1O_2$) produced by the PMS decomposition served as the major reactive species for the degradation of HA. An underlying synergistic adsorption and oxidation mechanism involving a local high concentration reaction region around the KBC interface was then proposed. This work not only provides a cost-effective solution for the elimination of HA but also advances our understanding of the nonradical oxidation at the biochar interface.

Humic acid (HA) is a polyphenolic substance that forms through the microbial decomposition of organic residues and a series of chemical processes, and is the primary component of humus [1]. While HA itself is non-toxic, it can affect the behavior of other contaminants in water environments. For example, it can react with halogens, act as a precursor to carcinogenic and mutagenic disinfection by-products, and inhibit the purification ability of disinfectants [2,3]. Previous researches in water treatment mainly focused on the influence of HA on disinfectants or the adsorption removal processes of HA [4]. Recently, AOPs have shown enormous application promise in degrading organic impurities in water. However, few investigations directly targeted HA as the pollutant of interest. Instead, HA was typically introduced as an influencing factor to assess the anti-interference ability of oxidation processes in most cases [5–7]. This, to some extent, reflected that HA could be degraded in AOPs. Therefore, it is necessary to explore the performance and mechanism of AOPs for the removal of HA in order to further ensure water safety.

In the last decade, peroxymonosulfate (PMS)-based AOPs have garnered widespread attention from the academic community. While activation methods based on metal catalysis are the most classical, they still have disadvantages such as metal leaching pollution and susceptibility to the water environment [8–11]. Metal-free heterogeneous catalysts for PMS activation have gradually become a topic of interest due to the lack of these problems [12]. Carbon materials were commonly studied as nonmetal activators for persulfate due to their controllable electronic structures and stable physicochemical properties [13]. Activation efficiency could be significantly improved through simple chemical modifications such as acid/alkali treatment and heteroatom doping [14,15]. Biochar, a solid product derived from the pyrolysis of waste biomass, on the one hand, was considered to be a cost-effective and environmentally friendly platform material for promoting the application of carbon-induced AOPs [16]. At this stage, there is a high demand for the development of biochar catalysts with high PMS activation performance.

* Corresponding author.
E-mail address: guowanqian@hit.edu.cn (W.-Q. Guo).

https://doi.org/10.1016/j.cclet.2024.110244
1001-8417/

Besides, insights into PMS activation processes on the biochar interface have been a hot topic of research for several years. Generally, oxidation of contaminants could be divided into radical and nonradical pathways. Radical pathways typically involved two reactive oxygen species (ROS): hydroxyl radical ($^{\bullet}OH$) and sulfate radical ($SO_4^{\bullet-}$), which could be derived from the dissociation of the peroxy bond of PMS. Nonradical pathways included singlet oxygenation and mediated electron transfer (MET) processes [17,18]. Although nonradical oxidation was thought to be milder and more selective than the radical pathway, the specific nonradical mechanism of PMS activation remains ambiguous [16]. For example, it was reported that singlet oxygen ($^1O_2$) could be produced by the reactions between ketone groups and PMS while the adsorption of organics was reported to play a critical role in the MET process [7,19]. In contrast, the possible contribution of adsorption was seldomly concerned in $^1O_2$ dominated PMS-based AOPs [19–21]. A previous study pointed out that there did exist a synergistic effect of pollutant adsorption and singlet oxygenation in the NiOOH/PMS system [22]. Therefore, we speculate that the excellent adsorption nature of biochar could facilitate the interaction between targeted organics and the *in-situ* generated $^1O_2$, thereby improving the oxidation efficiency of the entire system.

Alkali activation is one of the commonly employed chemical activation methods, which is expected to change the pore structure and meanwhile introduce more oxygen functional groups [23]. Herein, we investigated the modifying effect of alkali-activated calcination on the rice straw-derived biochar using various characterization methods. We then studied the performance and mechanism of the biochar/PMS system, targeting HA as the contaminant, from two aspects: adsorption and catalysis. Furthermore, we proposed an underlying synergistic degradation mechanism on the biochar interface. This work is expected to provide an efficient and feasible elimination scheme for HA, while also offering insights into biochar-induced singlet oxygenation processes. Experimental details can be found in the Supporting information.

Fig. S1 (Supporting information) present scanning electron microscope (SEM) images of the pristine biochar (BC) and alkali modified biochar (KBC), respectively. The alkali treatment caused damage to the carbon skeleton, resulting in a roughened surface and an increased number of surface pores. Some of the pores became unordered and random, which might provide more active sites. The N_2 adsorption-desorption isotherms and pore size distribution of BC and KBC are shown in Fig. 1a, both exhibiting type II isotherm curves, indicating the presence of micropores and mesopores. BET specific surface area increased from 369.7056 m^2/g of BC to 1281.6095 m^2/g of KBC, with an increase in pore volume and aperture size as well. The improved surface area and porosity of KBC might be due to the alkali corrosion and dissolution of the carbon skeleton and impurities. Moreover, the K element could increase the microporosity rate by entering the carbon lattice [23–25]. These results indicated that KBC might show better adsorption ability than BC.

X-ray diffraction (XRD) spectra were obtained to investigate the crystalline characteristics of BC and KBC. As shown in Fig. S2 (Supporting information), three peaks were observed at 14.5°, 29.1°, and 42.5°, corresponding to the (001), (002), and (100) lattice planes of graphite carbon, respectively [26]. This suggested that carbonization dissolved hemicellulose and lignin of straw, while cellulose was cleaved and lost H, O, and free C atoms. This resulted in the formation of microcrystalline carbon fiber through aromatization rearrangement reactions and eventually the formation of a graphitic structure. The graphitic structure did not significantly change after modification. Fourier transform infrared spectroscopy (FTIR) analysis (Fig. 1b) revealed that alkali treatment did not change the types of functional groups but their contents. The broad peaks observed at 3440 cm^{-1} were associated with -OH vibration, while the weak peaks between 2800 and 3000 cm^{-1} indicated $-CH_2$ vibration. The moderate peaks at 1583 cm^{-1} were attributed to C=O or C=C vibration, while the strong peaks observed at 1050 cm^{-1} represented C-OH vibration. Obviously, the intensities of C=O/C=C, C-OH, and $-CH_2$ increased after the modification. Additionally, the blue shift after treatment suggested that KBC had a stronger electrostatic attraction than BC at the interface [23,27].

X-ray photoelectron spectroscopy (XPS) analysis showed two peaks at binding energies of 285 and 533 eV, corresponding to C 1s and O 1s, respectively (Fig. 1c). These peaks indicated that C and O elements were the main constituents of both materials, and the content of O element increased markedly after treatment. Analysis of C 1s peaks in BC and KBC (Fig. 1d) revealed four components at around 285, 286, 288, and 290 eV, corresponding to C=C, C-O, C=O,

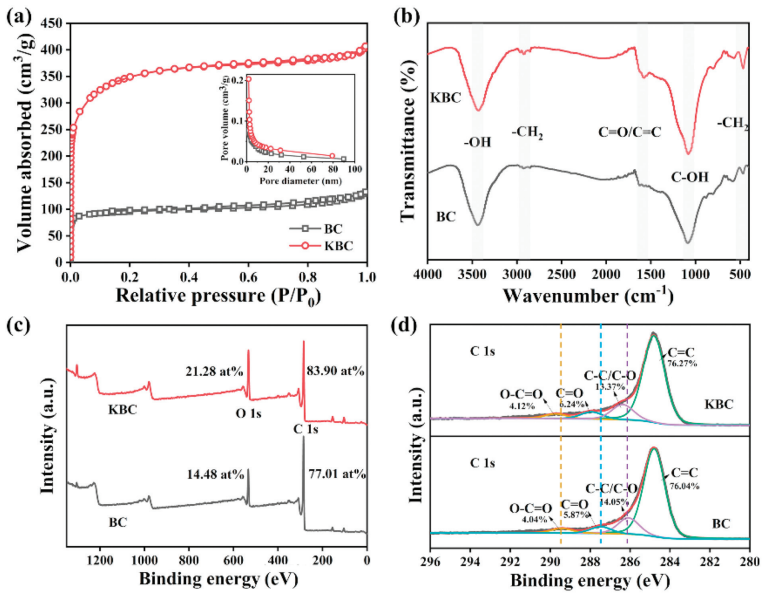

Fig. 1. (a) The N_2 adsorption-desorption isotherms and pore size distribution of BC and KBC. (b) FTIR analysis, (c) XPS survey, (d) high resolution C 1s spectra of BC and KBC.

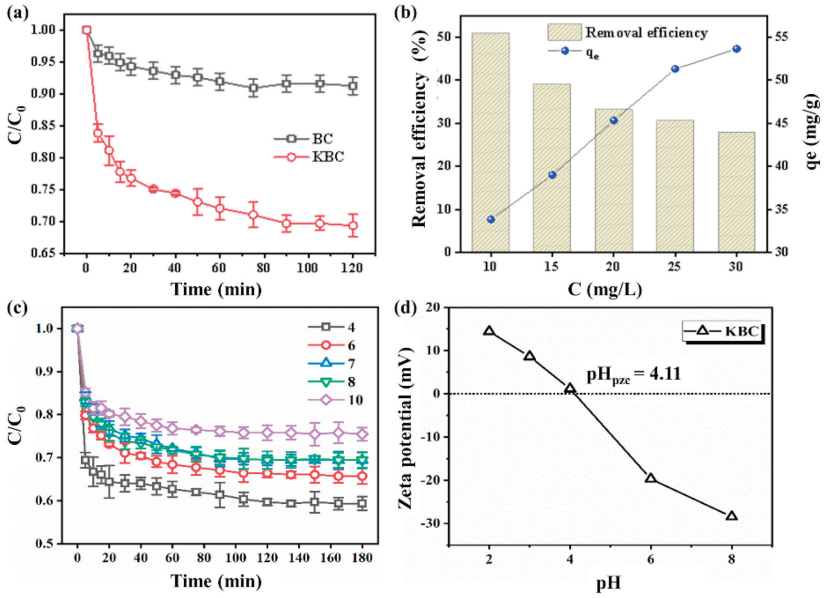

Fig. 2. (a) The adsorption performance of BC and KBC. (b) The influence of HA concentration on the removal and equilibrium adsorption capacity (q_e) by KBC. (c) The adsorption efficiency of HA on KBC at different pH conditions of the solution. (d) Electrical properties of KBC on the solution's pH values. Conditions: [HA] = 20 mg/L, [Catalyst] = 150 mg/L, initial pH 7, T = 25 °C.

and O=C-O groups, respectively [25,28]. The content of C=O in KBC increased compared to BC, which was consistent with the results of FTIR analysis. The characterization results indicated that the alkali-activated calcination treatment did not change the fundamental skeleton structure of BC, but significantly improved its pore structure and introduced more carbonyl functional groups, which was expected to facilitate the adsorption and oxidative degradation of HA.

Fig. 2a illustrated that the adsorption efficiency of BC was much weaker than that of KBC. The removal efficiency of BC on HA was merely 8.73%, which was 71.44% less than that of KBC (30.57% at 90 min). The improved adsorption capacity of KBC could be attributed to its increased specific surface area and well-developed pore structure [29–31]. Additionally, the abundance of C=O in KBC could promote physical or chemical interaction, thus facilitating the removal of HA [32]. The influence of concentration on the adsorption of HA by KBC was investigated (Fig. 2b). The results showed that the adsorption efficiency of KBC on HA decreased as the concentration of HA increased, while the equilibrium adsorption capacity (q_e) increased. Specifically, when the HA content was increased from 10 mg/L to 30 mg/L, the q_e increased by 58.40%, but the adsorption efficiency decreased by 45.09%. This could be attributed to the more intense competition for the available adsorption sites on KBC at higher concentrations of HA. The adsorption of HA on KBC was significantly influenced by the pH of the solution, as shown in Fig. 2c. As the pH increased, the adsorption efficiency was inhibited, and the HA removal efficiency decreased by 39.05% at pH 10 compared to pH 4. Fig. 2d illustrated that KBC displayed different electrical properties depending on the solution's pH values. KBC was electropositive at pH < 4.11 but became electronegative at pH > 4.11 due to deprotonation, indicating that electrostatic forces might play a role in adsorption [33]. The carboxyl and phenolic hydroxyl groups of HA made the most significant contribution to the molecular charge, and their deprotonation at pH >4 and pH >8 would increase the electronegativity of HA [34,35]. Therefore, increasing the pH was detrimental to the interaction in the system. On the other hand, a low pH could encourage HA to fold into a compact conformation and form a rigid spherical colloidal structure, leading to improved diffusion and adsorption. In a high pH environment, ionized HA would extend into a linear structure and increase in molecular size, inhibiting its adsorption on KBC [36,37].

The adsorption kinetics of HA onto KBC were analyzed using both the *pseudo*-first-order and the *pseudo*-second-order models, with the latter proving to be the better fit (Fig. 3a and Tables S1 and S2 in Supporting information), indicating the potential involvement of chemical adsorption in the removal process [38]. Additionally, the intra-particle diffusion model was applied to investigate the adsorption control steps (Text S6 in Supporting information). The resulting plot (Fig. 3b) displayed two distinct linear segments with R^2 values of 0.9944 and 0.9556 for the first and second stages, respectively, and corresponding constant K of the intra-particle diffusion rate valued 4.4672 and 0.9274 (mg·min$^{0.5}$)/g. The faster initial stage can be attributed to a higher concentration gradient and mass transfer rate, which facilitates HA diffusion into KBC. However, as the concentration gradient decreases in the solution, active surface sites become occupied, and pores become clogged, hindering further entry of HA. It is noteworthy that the curves did not intersect at the origin, implying that the intraparticle diffusion process was not the sole rate-limiting step [39].

Isotherm models were used to simulate the adsorption process, with the Langmuir isotherm equation showing a better fit to the experimental data (Fig. 3c and Tables S3 and S4 in Supporting information). This indicated that the adsorption process was mainly due to the formation of a monolayer. The complexity and variability of HA's chemical composition and structure, as well as its sensitivity to environmental factors, make it challenging to establish a comprehensive and precise adsorption model [37,40]. Theoretically, isotherm models are influenced by both the equilibrium concentration of the adsorbate and the concentration of the adsorbent. Isothermal parameters for HA adsorption onto KBC at different concentrations indicated that adsorption of low-concentration HA (10–40 mg/L) was better fitted with the Langmuir model, while adsorption of high-concentration HA (30–80 mg/L) was better fitted with the Freundlich model. This suggested that the adsorption process of KBC changed with the concentration of HA. Previous work suggested that there were two sites reacting at different stages on biochar: more active but fewer sites named A sites,

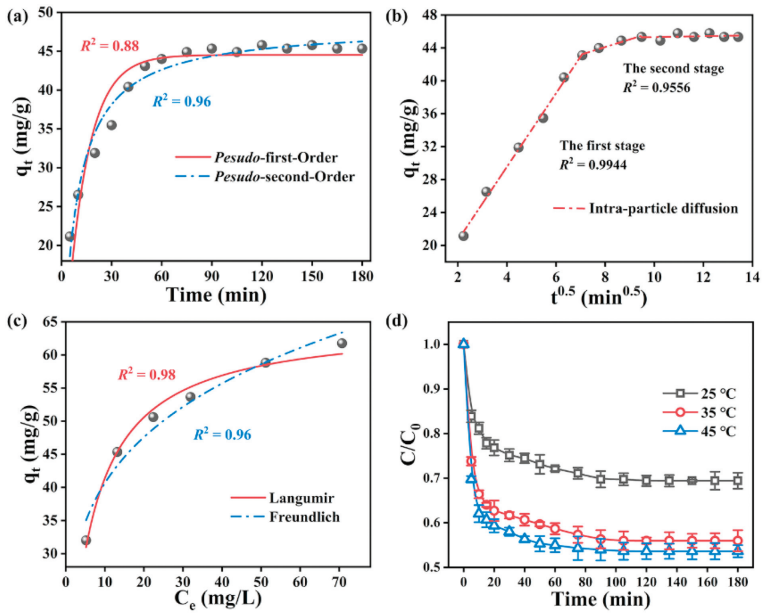

Fig. 3. (a) The *pseudo*-first-order and the *pseudo*-second-order models fitting the adsorption kinetics of HA onto KBC. (b) The intra-particle diffusion model of the adsorption control steps for the first and second stage. (c) Isotherm models of the adsorption process with the Langmuir and Freundlich isotherm equation. (d) The removal efficiency of HA on KBC at various temperatures. Conditions: [HA] = 20 mg/L, [Catalyst] = 150 mg/L, initial pH 7, T = 25 °C.

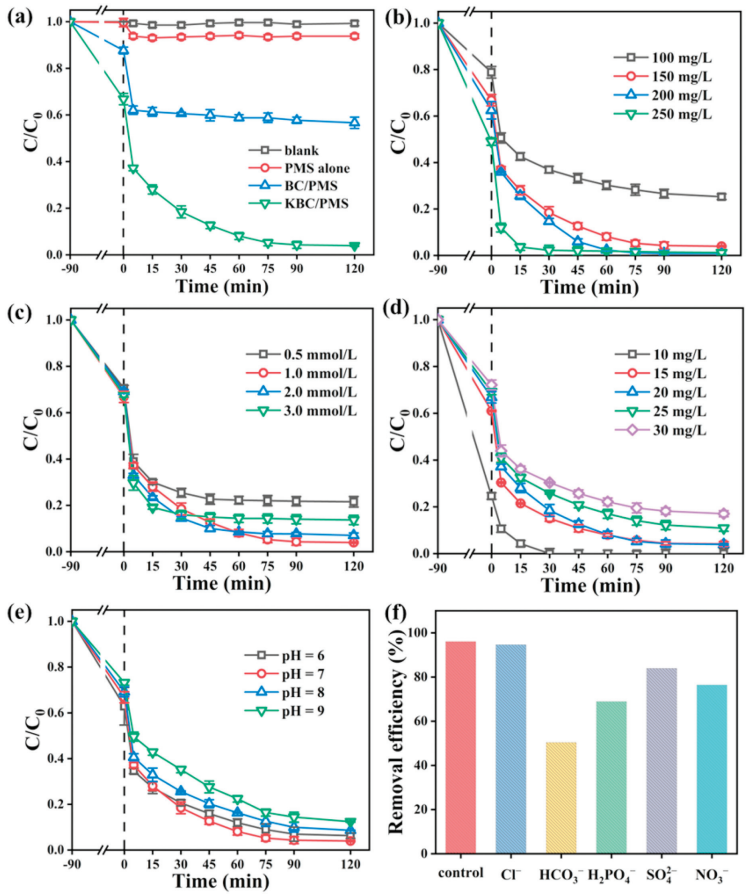

Fig. 4. (a) Degradation of HA in different systems. (b) Effect of KBC dosage, (c) effect of PMS concentration, (d) effect of HA concentration, (e) effect of initial pH, (f) effect of inorganic anions on the degradation efficiency of HA. Conditions: [HA] = 20 mg/L, [Catalyst] = 150 mg/L, [PMS] = 1.0 mmol/L, initial pH 7, [inorganic anions] = 1.0 mmol/L, T = 25 °C.

and numerous sites with lower activity named B sites [41]. B sites would be occupied until A sites were filled; thus, HA might occupy A sites of KBC in the first stage, which obeyed the Langmuir model. As the content of HA increased, A sites were filled and B sites were occupied in the second stage, which obeyed the Freundlich model.

Furthermore, the results from Fig. 3d demonstrated that the removal efficiency of HA was significantly enhanced with an increase in temperature. Specifically, the degradation rate of HA with a 45 °C treatment was found to increase by 51.68% in comparison to that with a 25 °C treatment. This enhancement could be attributed to the stimulated molecular diffusion in the system [42]. Moreover, the calculated adsorption thermodynamic parameters (ΔG, ΔH, and ΔS) were all negative (Text S7 and Table S5 in Supporting information). This indicated that the adsorption of HA on KBC was a spontaneous, exothermic, and entropy-decreasing process, implying that the adsorption process was mainly dominated by chemical adsorption. The above results demonstrated that the alkali-calcination process greatly enhanced the adsorption capacity of BC for HA, potentially facilitating further oxidative degradation of HA on the carbon surface.

Fig. 4a showed that PMS alone had little effect on HA degradation, but degradation rate increased significantly when combined with BC or KBC. KBC treatment resulted in HA almost complete degradation in 120 min, with rates 15.47 and 2.21 times higher than PMS alone and BC/PMS, respectively. The study on the influence of KBC content on HA degradation (Fig. 4b) showed that the degradation rate of HA increased with increasing KBC concentration. The degradation rate increased with increasing PMS concentration up to 1.0 mmol/L (Fig. 4c). However, higher PMS concentrations inhibited degradation, possibly due to extra PMS occupying adsorption sites or scavenging ROS [43]. The initial HA concentration also affected degradation, with higher concentrations resulting in lower degradation rates (Fig. 4d). This phenomenon can be explained in two ways. Firstly, the larger quantity of targeted pollutant present can directly influence the degradation kinetics due to the limited removal capacity of the KBC/PMS system. Secondly, the occupation of surface-active sites, such as those containing C=O groups, may hinder the production of ROS, thus impeding the degradation process. Fig. 4e showed that the degradation rate of HA in the KBC/PMS system initially increased and then decreased as the pH increased, reaching its peak at pH 7. Even at pH 9, the removal efficiency of HA in the KBC/PMS system was still above 80%, indicating the wide pH application range of the KBC/PMS system [44]. The presence of inorganic anions affected the HA degradation in the KBC/PMS system (Fig. 4f). HCO_3^- inhibited the reaction due to the increase in pH and transform of ROS, while $H_2PO_4^-$ hindered the removal of HA by occupying the active sites on KBC and scavenging ROS [7,45]. Cl^- can be easily oxidized by $^{\bullet}OH$ and $SO_4^{\bullet-}$ to produce chloride radicals ($Cl^{\bullet}$) with lower oxidizing ability [46]. However, Cl^- here negligibly inhibited the removal of HA, indicating that radical pathway was not the main oxidation pathway of HA.

To identify the dominant ROS involved in the KBC/PMS system, scavengers of $^{\bullet}OH$ and $SO_4^{\bullet-}$, $^{\bullet}OH$, $^{\bullet}O_2^-$, and $^1O_2$ namely MeOH, TBA, *p*-BQ, and FFA, were used [47,48]. The results, depicted in Fig. 5a, indicated that MeOH, TBA, and *p*-BQ slightly inhibited HA degradation, suggesting that the radical contribution was minimal. The significant inhibition caused by FFA supported the nonradical singlet oxygenation pathway as the major pathway. The contributions of different ROS were then quantified according to the pseudo-second-order kinetic model as 15.34% for $^{\bullet}O_2^-$, 14.46% for $SO_4^{\bullet-}$, 11.99% for $^{\bullet}OH$, and 58.20% for $^1O_2$ respectively (Text S8). The dominant role of $^1O_2$ was further confirmed through EPR detection using DMPO and TEMP as spin trappers. No free radical signal was detected using DMPO as the trapper, indicating a low contribution of free radicals [49]. An EPR experiment with TEMP as an active species trapping agent revealed a characteristic signal of three-lines corresponding to 2,2,6,6-tetramethylpiperidine-*N*-oxyl (TEMPO) in the ESR spectrum (Fig. 5b), which was attributed to TEMP-$^1O_2$ and indicated the self-decomposition of PMS. Notably, the intensity of the signal in the KBC/PMS system was significantly strengthened, providing evidence for the production of $^1O_2$ on the KBC surface. These results are consistent with previous findings indicating that the C=O on KBC can serve as the reactive sites for PMS activation, thereby initiating the singlet oxygenation of organic pollutants [47,49,50].

The results of the study showed that $^1O_2$ was the dominant ROS in the KBC/PMS system for HA degradation. However, according to kinetics calculations, the contribution of $^1O_2$ to the degradation of pollutants was only 0.22%, as its reaction rate constants

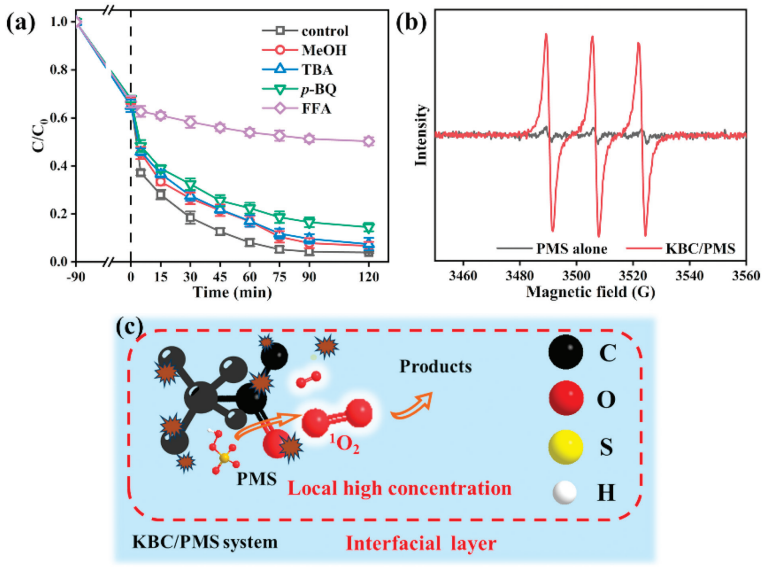

Fig. 5. (a) The HA degradation rates of radical quenching experiments in KBC/PMS systems. (b) EPR spectra with TEMP as trapping-agent in KBC/PMS system. (c) Mechanism of HA degradation in KBC/PMS system. Conditions: [HA] = 20 mg/L, [Catalyst] = 150 mg/L, [PMS] = 1.0 mmol/L, initial pH 7, [MeOH] = [TBA] = 1.0 mol/L, [*p*-BQ] = [FFA] = 5 mmol/L, T = 25 °C.

with water and HA were 1.2×10^8 and 2.65×10^5 L mol^{-1} s^{-1}, respectively, which conflicted with the experimental results [51,52]. Many studies have used this kinetics calculation to evaluate and exclude the domination of $^1O_2$, but it should be noted that the analysis is based on homogeneous systems, where $^1O_2$ is dispersed in water, and may not be applicable to heterogeneous systems. In this study, HA was concentrated on the KBC surface, and $^1O_2$ was formed *in situ*, which might provide the necessary conditions for contact and reaction between HA and $^1O_2$. As illustrated in Fig. 5c, HA degradation in the KBC/PMS system was suggested to be an adsorption-oxidation cooperative process, in which adsorption made the $^1O_2$-led oxidation process efficient and stimulated significant degradation of pollutants. Specifically, the more complex pore structure and oxygen functional groups on the modified KBC increased the enrichment of HA on the material surface significantly. PMS in the system was able to react with C=O of KBC and produce $^1O_2$ *in situ*, which oxidized HA adsorbed on the KBC surface immediately and achieved HA degradation [50].

To conclude, we found that the adsorption and activation capacities of BC were found to be drastically improved through an alkali-activated calcination process. The obtained KBC sample showed a porous structure, and with much more C=O groups introduced. Mechanism analysis results indicated that chemical adsorption and singlet oxygenation made major contribution to the HA removal on KBC. The enrichment of HA and *in-situ* generation of $^1O_2$ together created a local high concentration reaction region around the carbon interface, which to a large extent securing the oxidation efficiency. This work provides a cost-effective AOPs scheme for the removal of HA, and offers a new insight into the nonradical oxidation mechanism at the carbon interface.

Declaration of competing interest

The authors declare that they have no known competing financial interests or personal relationships that could have appeared to influence the work reported in this paper.

CRediT authorship contribution statement

Huazhe Wang: Writing – original draft, Visualization, Funding acquisition, Formal analysis, Conceptualization. **Chenghuan Qiao:** Writing – review & editing, Visualization, Investigation. **Chuchu Chen:** Writing – review & editing, Visualization, Methodology. **Bing Liu:** Writing – review & editing, Methodology, Investigation, Formal analysis. **Juanshan Du:** Writing – review & editing. **Qinglian Wu:** Writing – review & editing. **Xiaochi Feng:** Writing – review & editing. **Shuyan Zhan:** Writing – review & editing. **Wan-Qian Guo:** Writing – review & editing, Resources, Project administration.

Acknowledgments

This work was financially supported by the National Natural Science Foundation of China (No. 52200049), the China Postdoctoral Science Foundation (No. 2022TQ0089), and the Heilongjiang Province Postdoctoral Science Foundation (No. LBH-Z22181).

Supplementary materials

Supplementary material associated with this article can be found, in the online version, at doi:10.1016/j.cclet.2024.110244.

References

[1] C. Ma, M. Chen, H. Liu, et al., Chin. Chem. Lett. 29 (2018) 136–138.
[2] P. Zhang, X. Zhang, X. Zhao, et al., J. Hazard. Mater. 424 (2022) 127653.
[3] X. Zhu, J. Liu, L. Li, et al., Chemosphere 312 (2023) 137193.
[4] M.A. Islam, D.W. Morton, B.B. Johnson, et al., Sep. Purif. Technol. 247 (2020) 116949.
[5] Q. Si, W. Guo, H. Wang, et al., Chin. Chem. Lett. 31 (2020) 2556–2566.
[6] H.N. Tien, M.T. Duc, N.V. Thang, et al., Chemosphere 308 (2022) 136457.
[7] H. Wang, W. Guo, B. Liu, et al., Appl. Catal. B 279 (2020) 119361.
[8] X. Li, Z. Zhao, H. Li, et al., Chem. Eng. J. Adv. 8 (2021) 100143.
[9] Z. Zeng, A. Khan, Z. Wang, et al., Chem. Eng. J. 397 (2020) 125425.
[10] H. Yang, B. Luo, S. Lei, et al., Sep. Purif. Technol. 264 (2021) 118466.
[11] A.D. Bokare, W. Choi, J. Hazard. Mater. 275 (2014) 121–135.
[12] C. Dai, S. Li, Y. Duan, et al., Water Res. 216 (2022) 118347.
[13] N. Wang, W. Ma, Z. Ren, et al., J. Mater. Chem. A 6 (2018) 884–895.
[14] M. Kohantorabi, G. Moussavi, S. Giannakis, Chem. Eng. J. 411 (2021) 127957.
[15] H. Luo, W. Guo, Q. Zhao, et al., Chin. Chem. Lett. 33 (2022) 1293–1297.
[16] C. Zhao, B. Shao, M. Yan, et al., Chem. Eng. J. 416 (2021) 128829.
[17] Y.X. Guo, L.G. Yan, X.G. Li, et al., Sci. Total Environ. 783 (2021) 147102.
[18] M.M. Mian, G. Liu, Chem. Eng. J. 392 (2020) 123681.
[19] J. Wang, Z. Liao, J. Ifthikar, et al., Chemosphere 185 (2017) 754–763.
[20] D. Ding, L. Zhou, F. Kang, et al., ACS Appl. Mater. Interfaces 12 (2020) 53788–53798.
[21] X. Fan, H. Lin, J. Zhao, et al., Sep. Purif. Technol. 272 (2021) 118909.
[22] C. Lyu, L. Zhang, D. He, et al., Chin. Chem. Lett. 33 (2022) 930–934.
[23] N. An, M. Zhao, X. Zheng, et al., J. Hazard. Mater. 424 (2022) 127444.
[24] D. Zhu, J. Shao, Z. Li, et al., J. Hazard. Mater. 416 (2021) 125693.
[25] W. Wang, X. Ma, J. Sun, et al., Spectrosc. Lett. 52 (2019) 367–375.
[26] A.L. Cazetta, T. Zhang, T.L. Silva, et al., Appl. Catal. B 225 (2018) 30–39.
[27] V. Nguyen, T. Nguyen, C.P. Huang, et al., J. Water Process Eng. 40 (2021) 101908.
[28] H. Huang, Z. Huang, W. Zhou, Clean Technol. Environ. Policy 25 (2023) 10069–11077.
[29] D.V. Cuong, N. Liu, V.A. Nguyen, et al., Sci. Total Environ. 692 (2019) 844–853.
[30] F. Li, Y. Wan, J. Chen, et al., Chemosphere 260 (2020) 127566.
[31] D. Zheng, M. Wu, E. Zheng, et al., J. Colloid Interface Sci. 625 (2022) 596–605.
[32] F. Lian, B. Sun, X. Chen, et al., Environ. Pollut. 204 (2015) 306–312.
[33] J. Wang, Y. Zhou, A. Li, et al., J. Hazard. Mater. 176 (2010) 1018–1026.
[34] Z. Liu, S. Zhou, Water Sci. Technol. 2017 (2017) 16–26.
[35] K. Feng, Z. Xu, B. Gao, et al., Environ. Pollut. 290 (2021) 117992.
[36] S. Wang, Q. Ma, Z.H. Zhu, Fuel Process. Technol. 90 (2009) 375–380.
[37] K. Yang, J.T. Fox, J. Environ. Eng. 144 (2018) 04018104.
[38] C. Peiris, S.R. Gunatilake, T.E. Mlsna, et al., Bioresour. Technol. 246 (2017) 150–159.
[39] X. Jing, Y. Wang, W. Liu, et al., Chem. Eng. J. 248 (2014) 168–174.
[40] D. Doulia, C. Leodopoulos, K. Gimouhopoulos, et al., J. Colloid Interface Sci. 340 (2009) 131–141.
[41] F.A. Mardini, B. Legube, J. Hazard. Mater. 170 (2009) 744–753.
[42] X. Zhang, J. Tian, P. Wang, et al., J. Clean. Prod. 332 (2022) 130069.
[43] T. Song, Y. Gao, J. Ye, et al., Environ. Sci. Pollut. Res. 30 (2023) 27394–27408.
[44] T. Liu, K. Cui, C. Li, et al., Chemosphere 311 (2023) 137084.
[45] C. Wang, Y. Wang, Y. Yu, et al., Sep. Purif. Technol. 295 (2022) 121255.
[46] Y. Gao, Y. Chen, T. Song, et al., Sep. Purif. Technol. 300 (2022) 121857.
[47] H. Wang, W. Guo, B. Liu, et al., Water Res. 160 (2019) 405–414.
[48] Q. Wu, Y. Zhang, H. Liu, et al., Water Res. 224 (2022) 119022.
[49] H. Peng, R. Chen, N. Tao, et al., Environ. Sci. Pollut. Res. 29 (2022) 49267–49278.
[50] H. Meng, C. Nie, W. Li, et al., J. Hazard. Mater. 399 (2020) 123043.
[51] Y. Yang, G. Banerjee, G.W. Brudvig, et al., Environ. Sci. Technol. 52 (2018) 5911–5919.
[52] R.M. Cory, J.B. Cotner, K. McNeill, Environ. Sci. Technol. 43 (2009) 718–723.